

ORIGINAL RESEARCH

Open Access



Left ventricular function assessment using $^{123}\text{I}/^{99\text{m}}\text{Tc}$ dual-isotope acquisition with two semi-conductor cadmium–zinc–telluride (CZT) cameras: a gated cardiac phantom study

Tanguy Blaire^{1,2,3*}, Alban Bailliez^{1,2,3}, Fayçal Ben Bouallegue⁴, Dimitri Bellevre⁴, Denis Agostini^{2,4} and Alain Manrique^{2,4}

* Correspondence:

ta.blaire@gmail.com

¹Nuclear Medicine, UF 5881, Groupement des Hôpitaux de l'Institut Catholique de Lille, Lomme, France

²Normandie Univ, UNICAEN, Signalisation, électrophysiologie et imagerie des lésions d'ischémie-reperfusion myocardique, 14000 Caen, France
Full list of author information is available at the end of the article

Abstract

Background: The impact of increased energy resolution of cadmium–zinc–telluride (CZT) cameras on the assessment of left ventricular function under dual-isotope conditions ($^{99\text{m}}\text{Tc}$ and ^{123}I) remains unknown.

The Amsterdam-gated dynamic cardiac phantom (AGATE, Vanderwilt techniques, Boxel, The Netherlands) was successively filled with a solution of ^{123}I alone, $^{99\text{m}}\text{Tc}$ alone, and a mixture of ^{123}I and $^{99\text{m}}\text{Tc}$. A total of 12 datasets was acquired with each commercially available CZT camera (DNM 530c, GE Healthcare and DSPECT, Biosensors International) using both energy windows ($^{99\text{m}}\text{Tc}$ or ^{123}I) with ejection fraction set to 33, 45, and 60 %. End-diastolic (EDV) and end-systolic (ESV) volumes, ejection fraction (LVEF), and regional wall motion and thickening (17-segment model) were assessed using Cedars-Sinai QGS Software. Concordance between single- and dual-isotope acquisitions was tested using Lin's concordance correlation coefficient (CCC) and Bland–Altman plots.

Results: There was no significant difference between single- or simultaneous dual-isotope acquisition (^{123}I and $^{99\text{m}}\text{Tc}$) for EDV, ESV, LVEF, or segmental wall motion and thickening. Myocardial volumes using single- (^{123}I , $^{99\text{m}}\text{Tc}$) and dual-isotope (reconstructed using both ^{123}I and $^{99\text{m}}\text{Tc}$ energy windows) acquisitions were, respectively, the following: EDV (mL) 88 ± 27 vs. 89 ± 27 vs. 92 ± 29 vs. 90 ± 26 for DNM 530c ($p = \text{NS}$) and 82 ± 20 vs. 83 ± 22 vs. 79 ± 19 vs. 77 ± 20 for DSPECT ($p = \text{NS}$); ESV (mL) 40 ± 1 vs. 41 ± 2 vs. 41 ± 2 vs. 42 ± 1 for DNM 530c ($p = \text{NS}$) and 37 ± 5 vs. 37 ± 1 vs. 35 ± 3 vs. 34 ± 2 for DSPECT ($p = \text{NS}$); LVEF (%) 52 ± 14 vs. 51 ± 13 vs. 53 ± 13 vs. 51 ± 13 for DNM 530c ($p = \text{NS}$) and 52 ± 16 vs. 54 ± 13 vs. 54 ± 14 vs. 54 ± 13 for DSPECT ($p = \text{NS}$); regional motion (mm) 6.72 ± 2.82 vs. 6.58 ± 2.52 vs. 6.86 ± 2.99 vs. 6.59 ± 2.76 for DNM 530c ($p = \text{NS}$) and 6.79 ± 3.17 vs. 6.81 ± 2.75 vs. 6.71 ± 2.50 vs. 6.62 ± 2.74 for DSPECT ($p = \text{NS}$). The type of camera significantly impacted only on ESV ($p < 0.001$).

(Continued on next page)

(Continued from previous page)

Conclusions: The new CZT cameras yielded similar results for the assessment of LVEF and regional motion using different energy windows (^{123}I or $^{99\text{m}}\text{Tc}$) and acquisition types (single vs. dual). With simultaneous dual-isotope acquisitions, the presence of ^{123}I did not impact on LVEF assessment within the $^{99\text{m}}\text{Tc}$ energy window for either CZT camera.

Keywords: CZT, SPECT, Myocardial perfusion imaging, Myocardial innervation imaging, Dual-isotope acquisition, mIBG, Dynamic phantom, DNM 530c, DSPECT

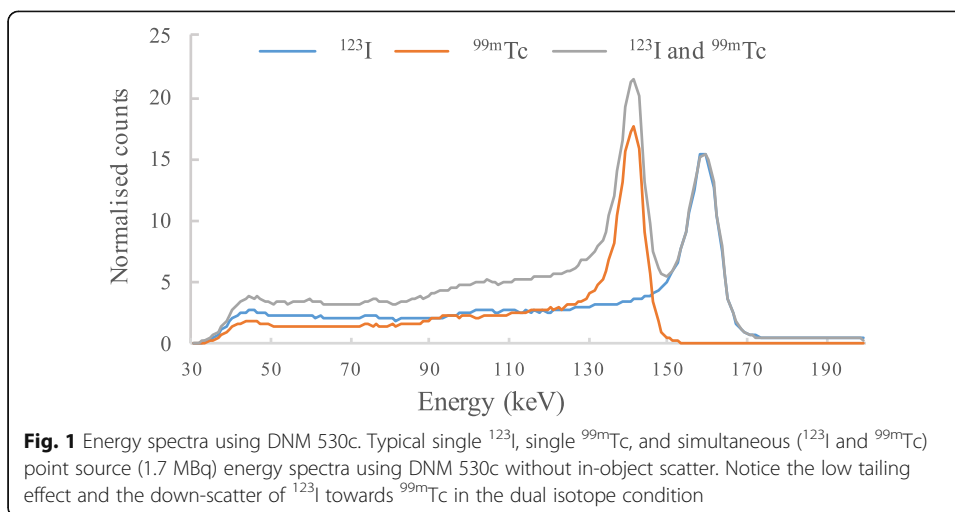
Background

The measurement of left ventricular (LV) ejection fraction (LVEF), end-diastolic volume (EDV), and end-systolic volume (ESV) using cardiac SPECT has been widely validated in comparison to other imaging techniques [1, 2]. Gated perfusion SPECT with $^{99\text{m}}\text{Tc}$ -labelled tracer is commonly used for prognosis assessment and clinical decision-making [3]. In addition, cardiac sympathetic innervation can be directly imaged with ^{123}I -meta-iodobenzylguanidine (^{123}I -mIBG), a radiolabelled norepinephrine analogue [4] that reflects neuronal integrity by visualising reuptake and retention in cardiac sympathetic terminals [5]. Previous studies using serial ^{123}I -mIBG and ^{201}Tl acquisitions have suggested that myocardial sympathetic innervation is compromised after myocardial infarction [6–8]. Due to the enhanced sensitivity of neural tissue to ischemia, regional sympathetic denervation exceeds the extent of the perfusion defect [9]. Comparing sympathetic innervation and viability is of potential interest to assess the risk of ventricular arrhythmias after myocardial infarction (MI) [10, 11].

The new cadmium–zinc–telluride (CZT) detectors offer higher photon sensitivity and dramatically increased spatial energy resolution compared with standard cameras. The advanced technical capabilities of these dedicated cardiac cameras enable combined assessment of myocardial innervation and perfusion within a single imaging session, using a dual injection of ^{123}I -mIBG and a $^{99\text{m}}\text{Tc}$ -labelled perfusion tracer. Bellevre et al. [12] recently demonstrated the feasibility of determining heart-to-mediastinum ratio of ^{123}I -mIBG uptake in patients with heart failure using dual-isotope imaging with a CZT camera (DSPECT) and combined $^{99\text{m}}\text{Tc}$ -tetrofosmin injection to localise the heart within the thorax.

Despite their increased energy resolution, the scatter fraction remains high with CZT cameras (30 vs. 34 % with conventional Anger gamma cameras) [13]. Moreover, the tailing effect in the energy spectrum towards lower energies due to incomplete charge collection [14] (Fig. 1) may specifically affect count statistics with CZT cameras. These two phenomena may impact on image acquisition within the $^{99\text{m}}\text{Tc}$ photopeak during a $^{123}\text{I}/^{99\text{m}}\text{Tc}$ dual-isotope acquisition, further compromising the accuracy of ventricular function assessment using gated SPECT with $^{99\text{m}}\text{Tc}$ -labelled tracer. This situation remains however to be investigated.

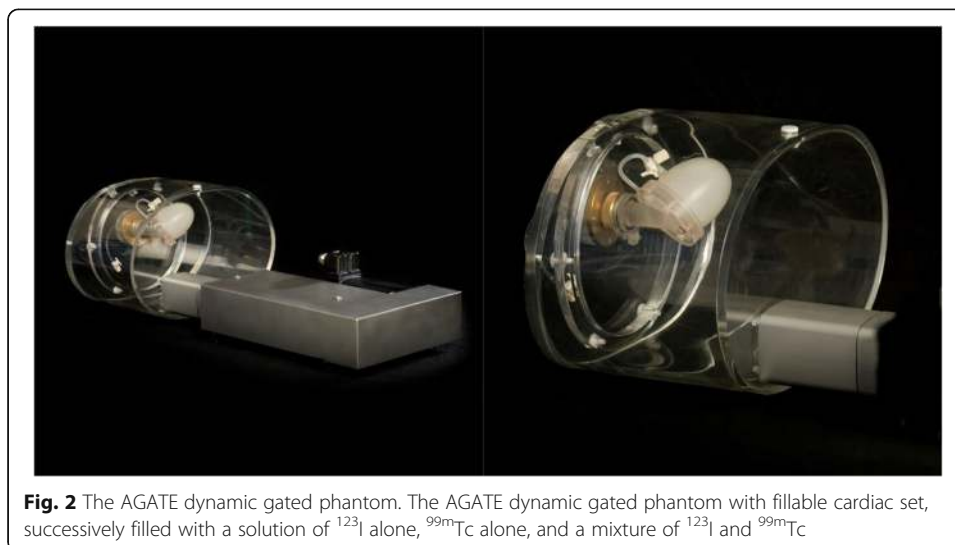
The aim of this study was to evaluate the impact of simultaneous dual-isotope ($^{123}\text{I}/^{99\text{m}}\text{Tc}$) acquisition on the assessment of global and regional left ventricular function in the $^{99\text{m}}\text{Tc}$ photopeak using two commercially available CZT cameras, Discovery NM 530c (DNM 530c, GE Healthcare, Milwaukee, WI, USA) and DSPECT (Biosensors International, Caesarea, Israel).



Methods

Gated phantom studies

We used the Amsterdam gated (Agate) dynamic phantom (Vanderwilt techniques, Boxtel, The Netherlands) as a reference for volume and LVEF measurements [15]. This phantom is a realistic 3-D water-filled torso with two thin membranes simulating endocardial and epicardial walls with known ejection fraction (Fig. 2). The compartment between these membranes was successively filled with a solution of ^{123}I alone, $^{99\text{m}}\text{Tc}$ alone, and a mixture of ^{123}I and $^{99\text{m}}\text{Tc}$ (22/44 kBq/mL, respectively) simulating the myocardial wall. The cardiac phantom stroke volume was controlled by a programmable adjustable pumping system, and an ECG-triggered signal was produced at a constant heart rate. Four datasets (single ^{123}I , single $^{99\text{m}}\text{Tc}$, dual ^{123}I , and $^{99\text{m}}\text{Tc}$) were acquired using three different ejection fractions (33 and 45 % to mimic LV dysfunction and 60 % to simulate normal LV function) on each camera (DNM 530c and DSPECT) with the following parameters: 10-min acquisition and 70-bpm contraction



rate. EDV, ESV, LVEF, and regional wall thickening and motion (17-segment model) were assessed using Quantitative Gated SPECT software (QGS, Cedars-Sinai Medical Center, Los Angeles, CA). The acquisition parameters were as follows: 70×70 matrix for the DNM 530c system and 64×64 for the DSPECT with a total of 120 projections recorded by each block in the heart area defined on a short prescan acquisition [13]. The energy window was asymmetric for both cameras, 140 keV ($-10 + 5$ %) for ^{99m}Tc and 159 keV ($-5 + 10$ %) for ^{123}I , for each acquisition.

CZT cameras

We successively used (i) a DNM 530c equipped with a multiple pinhole collimator and 19 stationary CZT detectors that simultaneously image 19 cardiac views, each detector being composed of four 5-mm-thick elements of 32×32 pixels (pixel size 2.46×2.46 mm) [16] and (ii) a DSPECT operating with nine mobile blocks of pixelated CZT detectors (pixel size 2.46×2.46 mm) associated with a wide-angle square-hole tungsten collimator, recording a total of 120 projections by each block [13]. All SPECT data were acquired and reconstructed using the parameters currently recommended for clinical routine and provided by each manufacturer, leading to a reconstructed pixel size of $4 \times 4 \times 4$ and $4.92 \times 4.92 \times 4.92$ mm for DNM 530c and DSPECT, respectively. No attenuation correction was performed.

Statistical analysis

Values are presented as mean \pm SD. A linear model analysis evaluated the effect of camera, acquisition type (single- vs. dual-isotope), isotope (^{123}I vs. ^{99m}Tc), and the interaction between camera type and isotope. Continuous mean values were compared using the Wilcoxon signed-rank test or Mann–Whitney U test when appropriate. Relationship between DNM 530c and DSPECT results were assessed using Pearson's (r) correlation coefficient, Bland–Altman limit-of-agreement, and Lin's concordance correlation coefficient (CCC), a measure of both precision and bias [17, 18]. Lin's CCC measures the equivalence of two measurement methods. The accuracy (i.e. the deviation of the best fit line from the line of identity) was assessed using the bias correction factor calculated as $C.b = CCC/r$, r being Pearson's correlation coefficient. The values of r and CCC were characterised using the Landis and Koch scale (0.2–0.4: fair; 0.4–0.6: moderate; 0.6–0.8: substantial; 0.8–1.0: almost perfect) [19]. A p value < 0.05 was considered statistically significant.

Statistical analyses were performed using R software (R Foundation for Statistical Computing, version 3.2.4, Vienna, Austria) except the linear model analysis performed using JMP 11 (SAS institute, Cary, NC).

Results

The mean values of overall cardiac volumes (EDV and ESV), LVEF, and regional wall motion and thickening using single- and dual-isotope acquisitions with DNM 530c and DSPECT are shown in Table 1 and illustrated in Figs. 3 and 4.

Linear model analysis demonstrated that the type of camera but not the acquisition mode (i.e. single- or dual-isotope) impacted on volume measurements. Post hoc Mann–Whitney test showed that this impact was only observed for the ESV

Table 1 Results for each camera

Camera	DNM 530c				DSPECT			
	¹²³ I		^{99m} Tc		¹²³ I		^{99m} Tc	
Energy window								
Acquisition type	Single	Dual	Single	Dual	Single	Dual	Single	Dual
EDV (mL)	88 ± 27	92 ± 29	89 ± 27	90 ± 26	82 ± 20	79 ± 19	83 ± 22	77 ± 20
ESV (mL)	40 ± 1*	41 ± 2*	41 ± 2*	42 ± 1*	37 ± 5	35 ± 3	37 ± 1	34 ± 2
LVEF (%)	52 ± 14	53 ± 13	51 ± 13	51 ± 13	52 ± 16	54 ± 14	54 ± 13	54 ± 13
Motion (mm)	6.72 ± 2.82	6.86 ± 2.99	6.58 ± 2.52	6.59 ± 2.76	6.79 ± 3.17	6.71 ± 2.50	6.81 ± 2.75	6.62 ± 2.74
Thickening (%)	47.7 ± 30.6	47.1 ± 29.9	45.4 ± 27.7	44.3 ± 29.2	44.2 ± 28.8	42.7 ± 23.6	42.2 ± 24.5	41.5 ± 26.7

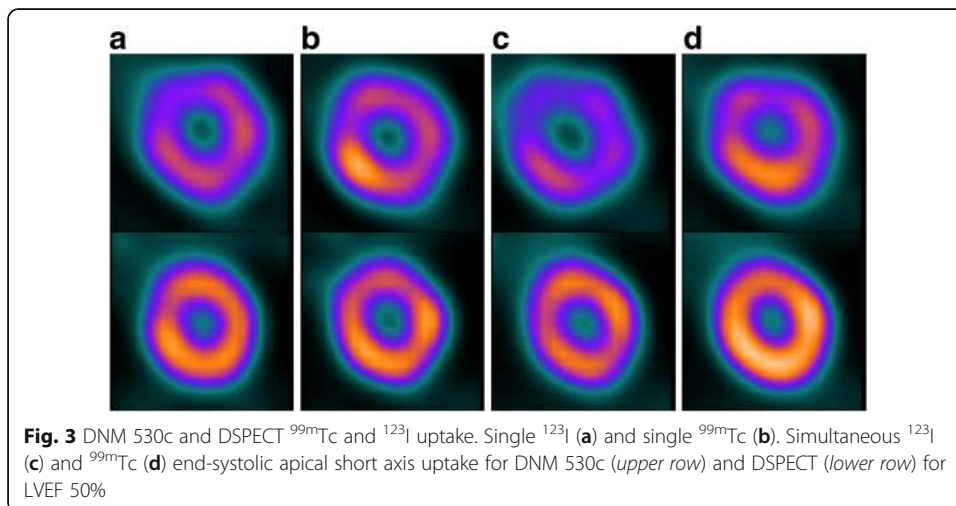
Phantom study results for each camera model expressed as mean ± SD. EDV, ESV, LVEF, and thickening and motion mean values for ^{99m}Tc and ¹²³I isotope in two acquisition types (single or dual), for both energy windows (¹²³I and ^{99m}Tc) on each camera (DNM 530c and DSPECT). **p* < 0.0001 vs. DSPECT

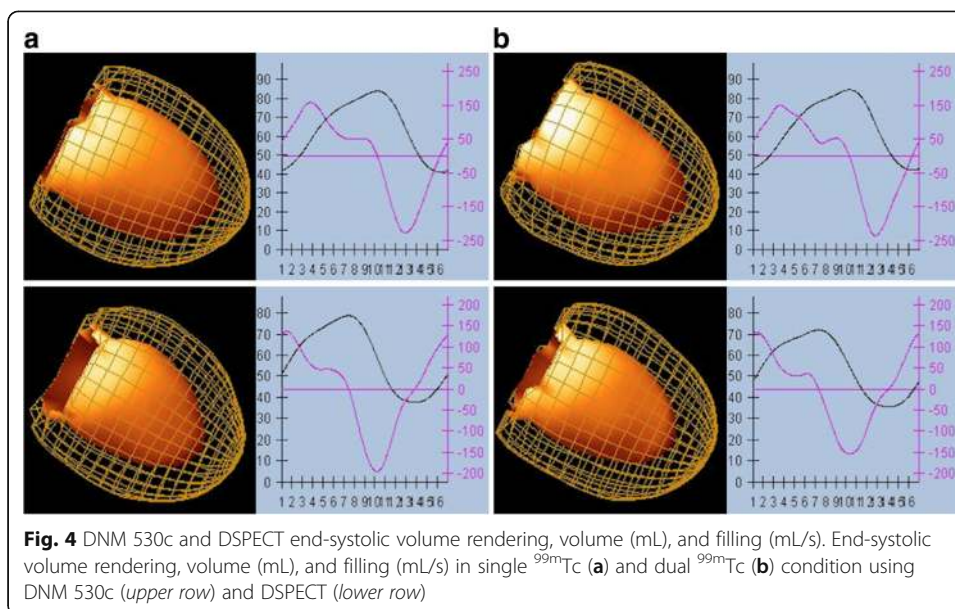
measurements (*p* < 0.0001) whereas EDV, LVEF, and segmental wall motion were similar for the two cameras.

Lin’s concordance correlation coefficient and Bland–Altman plots (see Tables 2 and 3 and Fig. 5) revealed an almost perfect agreement between single- and dual-isotope acquisitions for assessing segmental wall motion and thickening with ^{99m}Tc with both CZT cameras. Conversely, using ¹²³I, the agreement was weaker with both CZT cameras, with a decreased CCC and an increased 95 % CI of the difference between the two measurements on Bland–Altman plots. Pearson’s correlation (*r*) and CCC were similar, also indicating that no systematic bias was present (*C.b* > 0.97) between the two cameras and the acquisition mode.

Discussion

Our results demonstrated the feasibility of LVEF evaluation using gated perfusion SPECT with CZT cameras. On simultaneous dual radionuclide acquisitions, the ^{99m}Tc photopeak was unaffected by ¹²³I scatter and crosstalk. To our knowledge, this is the first dual-isotope gated phantom study evaluating ventricular function using the two commercially available CZT cameras (DNM 530c and DSPECT).





Dual-isotope acquisition with CZT cameras remains a challenging technique. Impaired myocardial innervation leads to low myocardial ¹²³I-mIBG uptake, requiring a dual-isotope protocol to localise the heart [12]. Due to the small field-of-view of the dedicated CZT cardiac cameras, a scout view is mandatory to localise the heart and correctly centre the field-of-view prior to SPECT acquisition. In addition, most of the patients referred for ¹²³I-mIBG assessment have an ischemic cardiomyopathy with heart failure (66 % in the ADMIRE-HF study [20]). In this clinical setting, the dual-isotope protocol allows a simple and efficient co-registration of innervation and perfusion studies and thus a robust assessment of innervation-perfusion mismatch. The measurement of LV function is a key step of prognosis assessment and may potentially be altered when using CZT cameras with a simultaneous dual-isotope protocol due to the down-scatter, crosstalk, and tailing effect of ¹²³I in the ^{99m}Tc photopeak.

Table 2 DNM 530c and DSPECT concordance correlation coefficients for motion

Motion		Pearson's	CCC [95 % CI]		Bland Altman		<i>R</i> ²	
		<i>r</i> [95 % CI]		C.b	Mean diff. [95 % CI]	Regression		
Acquisition	Isotope							
	Single	¹²³ I	0.94 [0.89–0.96]	0.93 [0.89–0.96]	0.99	0.06 [–2.15;2.28]	<i>y</i> = 0.123 <i>x</i> – 0.764	0.107
		^{99m} Tc	0.95 [0.92–0.97]	0.94 [0.91–0.97]	0.99	0.23 [–1.48;1.94]	<i>y</i> = 0.088 <i>x</i> – 0.354	0.071
Dual	¹²³ I	0.90 [0.83–0.94]	0.88 [0.81–0.93]	0.98	–0.15 [–2.8;2.5]	<i>y</i> = –0.188 <i>x</i> + 1.13	0.144	
	^{99m} Tc	0.94 [0.90–0.97]	0.94 [0.9–0.97]	1	0.03 [–1.81;1.87]	<i>y</i> = –0.007 <i>x</i> + 0.076	0	
Camera								
DSPECT	¹²³ I	0.91 [0.86–0.95]	0.89 [0.83–0.93]	0.98	0.08 [–2.57;2.72]	<i>y</i> = 0.248 <i>x</i> – 1.599	0.271	
	^{99m} Tc	0.97 [0.95–0.98]	0.97 [0.95–0.98]	1	0.22 [–1.74; 2.18]	<i>y</i> = –0.003 <i>x</i> + 0.239	0	
DNM 530c	¹²³ I	0.94 [0.90–0.97]	0.94 [0.9–0.97]	1	–0.14 [–2.11;1.84]	<i>y</i> = –0.061 <i>x</i> + 0.276	0.031	
	^{99m} Tc	0.97 [0.96–0.99]	0.97 [0.95–0.98]	1	–0.01 [–1.29;1.26]	<i>y</i> = –0.089 <i>x</i> + 0.576	0.135	

Bland–Altman mean difference (mean diff), regression, and *R*²
r, Pearson's correlation (*precision*); CCC, Lin's concordance correlation; C.b, *r*/CCC = bias factor (*trueness*)

Table 3 DNM 530c and DSPECT concordance correlation coefficients for thickening

Thickening		Pearson's	Bland Altman				
		<i>r</i> [95 % CI]	CCC [95 % CI]	C.b	Mean diff. [95 % CI]	Regression	<i>R</i> ²
Acquisition	Isotope						
Single	¹²³ I	0.93 [0.88–0.96]	0.92 [0.86–0.95]	0.99	−3.59 [−26.45;19.28]	<i>y</i> = −0.063 <i>x</i> − 0.694	0.026
	^{99m} Tc	0.94 [0.90–0.97]	0.93 [0.89–0.96]	0.99	−3.14 [−21.65;15.38]	<i>y</i> = −0.125 <i>x</i> + 2.331	0.121
Dual	¹²³ I	0.87 [0.79–0.93]	0.84 [0.75–0.9]	0.97	−4.35 [−33.78;25.08]	<i>y</i> = −0.248 <i>x</i> + 6.801	0.191
	^{99m} Tc	0.94 [0.90–0.97]	0.94 [0.89–0.96]	1	−2.84 [−22.04;16.35]	<i>y</i> = −0.09 <i>x</i> + 1.009	0.067
Camera							
DSPECT	¹²³ I	0.88 [0.80–0.93]	0.88 [0.81–0.93]	1	1.43 [−23.87;26.74]	<i>y</i> = 0.208 <i>x</i> − 7.608	0.177
	^{99m} Tc	0.96 [0.93–0.98]	0.96 [0.93–0.98]	1	0.78 [−14.06;15.63]	<i>y</i> = −0.088 <i>x</i> + 4.449	0.09
DNM 530c	¹²³ I	0.91 [0.85–0.95]	0.91 [0.85–0.95]	1	0.67 [−24.38;25.71]	<i>y</i> = 0.026 <i>x</i> − 0.588	0.004
	^{99m} Tc	0.96 [0.94–0.98]	0.96 [0.93–0.98]	1	1.08 [−14.5;16.65]	<i>y</i> = −0.053 <i>x</i> + 3.446	0.037

Bland–Altman mean difference (mean diff), regression, and *R*²
r, Pearson's correlation (*precision*); CCC, Lin's concordance correlation; C.b, *r*/CCC = bias factor (*trueness*)

Our results demonstrated that DNM 530c provided higher systolic volumes compared to the DSPECT camera. This camera effect on volume assessment is likely related to spatial resolution. Imbert et al. [21] reported the following classification of measured central spatial resolution: DNM 530c (6.7 mm) and DSPECT (8.6 mm). These results are concordant with previous findings by Bailliez et al. [22] showing in both phantom and patients that LV volumes were higher using the DNM 530c model compared to DSPECT and to Anger camera equipped with cardiofocal collimators.

Our results also demonstrated that, in comparison with single ^{99m}Tc acquisition, dual ¹²³I/^{99m}Tc acquisition did not compromise the assessment of ventricular function using the ^{99m}Tc photopeak. In some patients with severe heart failure, the sole use of ¹²³I-mIBG SPECT can lead to suboptimal localisation of the heart because of the CZT camera's narrow field-of-view, particularly when cardiac mIBG uptake is very low and the left ventricle is dilated. A dual-isotope protocol acquisition using both perfusion and innervation tracers provides a clear perfusion image and a perfect registration that allows the definition of the heart contours and thus an accurate measurement of ¹²³I-mIBG uptake [12].

In the clinical setting, simultaneous dual-radionuclide acquisition provides perfectly registered functional images leading to a reduced imaging time. In cardiac SPECT, several dual-radionuclide imaging protocols have been proposed. Simultaneous ^{99m}Tc-sestamibi/¹²³I-BMIPP imaging was proposed for assessing rest perfusion and fatty acid metabolism at the same time in patients with recent myocardial infarction [23, 24]. The dual-isotope acquisition protocol using ²⁰¹Tl and ¹²³I-mIBG is well documented on conventional Anger cameras, using the triple-energy window [25] for scatter and crosstalk correction. Simultaneous perfusion and sympathetic innervation imaging with ¹²³I-mIBG and ^{99m}Tc-labelled tracers enables the evaluation of innervation-flow mismatch and may provide valuable information to target the trigger zone in the setting of ventricular arrhythmia [4, 26]. In a recent study, Gimelli et al. [11, 27] using sequential ¹²³I-mIBG and ^{99m}Tc-tetrofosmin myocardial SPECT demonstrated a relevant association between innervation derangement (¹²³I-mIBG) and myocardial synchronicity (^{99m}Tc-tetrofosmin).

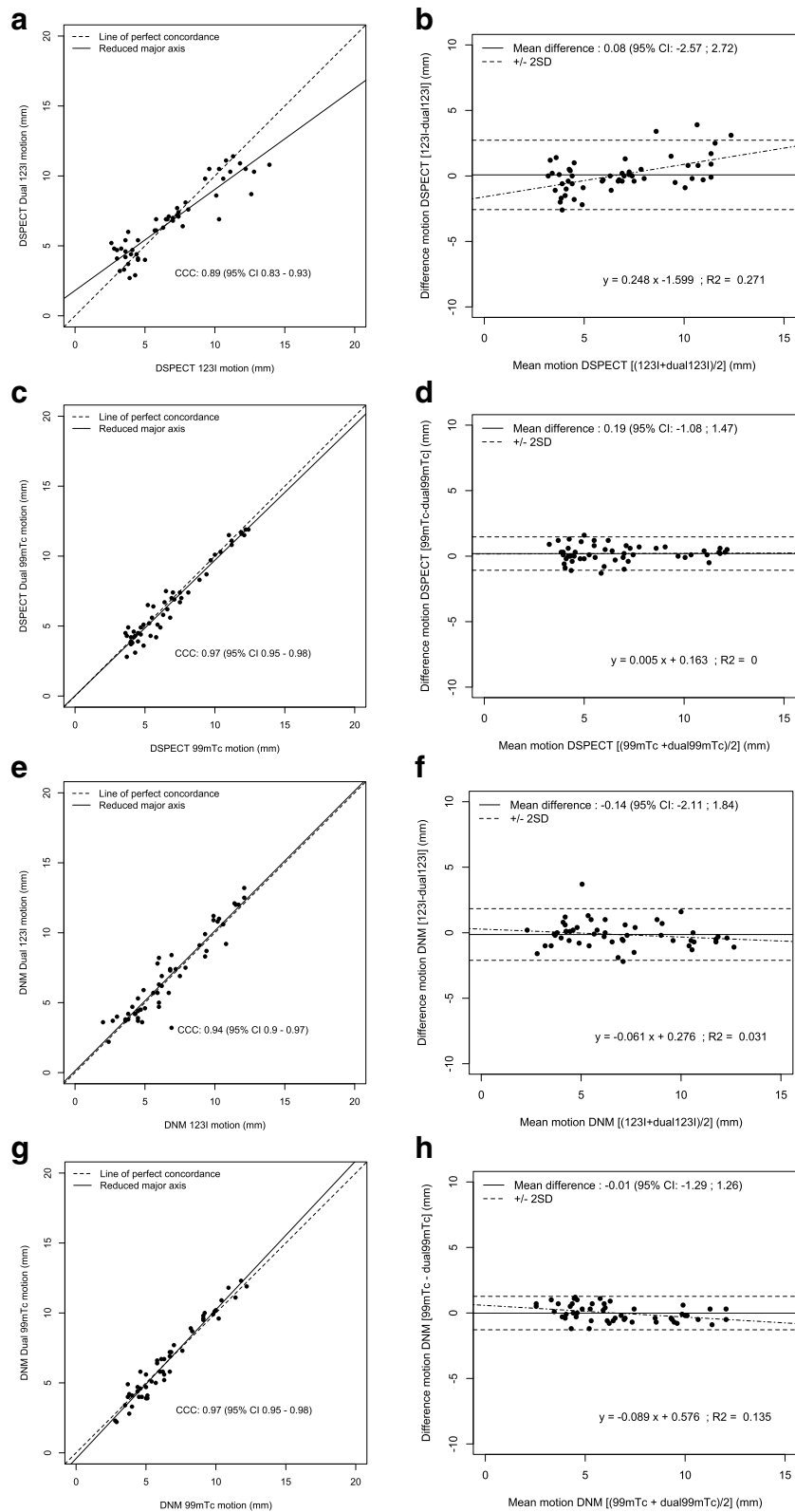


Fig. 5 Lin's CCC and Bland–Altman motion for DNM 530c and DSPECT. Lin's CCC for DSPECT ¹²³I (a) and ^{99m}Tc (c), DNM 530c ¹²³I (e), and ^{99m}Tc (g) motion and Bland–Altman plots for DSPECT ¹²³I (b) and ^{99m}Tc (d), DNM 530c ¹²³I (f), and ^{99m}Tc (h) motion for single and dual acquisitions

Despite a significant increase in energy resolution and sensitivity, the scatter fraction with the CZT camera is still high, evaluated up to 30 vs. 34 % with conventional Anger cameras [13]. Due to incomplete charge collection and intercrystal scatter, the CZT detectors are subjected to a tailing effect below the photopeak that may lead to an overcorrection of photon scatter when using a conventional triple-energy window method [28]. Recently, Fan et al. for the DNM 530c [29] and Holstensson et al. for the DSPECT [30] presented a model-based correction algorithm which extracts the useful primary counts of ^{99m}Tc and ^{123}I from projection data, taking into account the tailing effect to correct the scatter and crosstalk in ^{99m}Tc - ^{123}I dual imaging. In the present study, we did not apply any tailing effect correction and observed no significant impact on ventricular function assessment.

All reconstructions were performed using the vendor's workstation and available software for both cameras. Routinely, scatter and crosstalk correction is not performed on the DNM 530c camera. Image data from DSPECT were corrected for scatter and crosstalk but not for the tailing effect. In our study, the ratio between ^{123}I and ^{99m}Tc concentration was set to 1:2, which is representative of the low ^{123}I -mIBG myocardial uptake, observed in severe heart failure. Under these specific conditions, the absence of scatter and crosstalk correction using the DNM 530c did not affect ventricular function assessment using ^{99m}Tc acquisitions. In severe heart failure, ^{123}I -mIBG myocardial uptake is low and we assumed that the crosstalk and scatter of ^{123}I in the ^{99m}Tc photopeak had no consequences.

Limitations of the study

Due to the design of the phantom, EDV and ESV were not predetermined. The phantom was filled under static equilibrium conditions at atmospheric pressure to provide a reproducible ejection fraction. Based on this equilibrium, ejection fraction was imposed by injecting a stroke volume into the ventricular cavity [15, 22]. As a consequence, true EDV and ESV were not known and thus could not be compared with measured volumes.

As we used only commercially available software, scatter and crosstalk were corrected with DSPECT but not with DNM 530c. However, our results displayed no critical differences between the single-isotope and dual-isotope ^{99m}Tc window, even with the DNM 530c. At best, the demonstration could be made by comparing the results obtained with and without scatter and crosstalk corrections. However, the aim of our study was to compare the results obtained with the two CZT cameras using the dedicated commercially available software to mimic routine clinical conditions.

Conclusions

In this phantom study, the two CZT cameras (DNM 530c and DSPECT) provided similar results for ventricular function assessment (EDV, ESV, and LVEF) with single- (separate ^{123}I and ^{99m}Tc acquisitions) and simultaneous dual-isotope (^{123}I and ^{99m}Tc) acquisitions. Further studies are needed to evaluate perfusion match and mismatch using ^{123}I -mIBG and ^{99m}Tc -labelled tracers.

Acknowledgements

The authors thank Nathaniel Roth for his technical assistance. This work was conducted as part of the FHU REMOD-VHF project.

Authors' contribution

TB and AM: design of the study, data acquisition, analysis and interpretation of data, drafting of manuscript. AB and DB: data acquisition, analysis of data, and drafting of manuscript. FBB: statistical analysis, analysis of data and critical revision. DA: interpretation of data, drafting of manuscript. All authors read and approved the final manuscript.

Competing interests

The authors declare that they have no competing interests.

Author details

¹Nuclear Medicine, UF 5881, Groupement des Hôpitaux de l'Institut Catholique de Lille, Lomme, France. ²Normandie Univ, UNICAEN, Signalisation, électrophysiologie et imagerie des lésions d'ischémie-reperfusion myocardique, 14000 Caen, France. ³Nuclear Medicine, IRIS, Hôpital Privé Le Bois, 144 avenue de Dunkerque, 59000 Lille, France. ⁴Nuclear Medicine, CHU Cote de Nacre, Caen, France.

Received: 29 June 2016 Accepted: 1 November 2016

Published online: 11 November 2016

References

- Hachamovitch R, Berman DS, Kiat H, Cohen I, Friedman JD, Shaw LJ. Value of stress myocardial perfusion single photon emission computed tomography in patients with normal resting electrocardiograms: an evaluation of incremental prognostic value and cost-effectiveness. *Circulation*. 2002;105(7):823–9.
- Marcassa C, Bax JJ, Bengel F, Hesse B, Petersen CL, Reyes E, et al. Clinical value, cost-effectiveness, and safety of myocardial perfusion scintigraphy: a position statement. *Eur Heart J*. 2008;29(4):557–63.
- Thomas GS, Miyamoto MI, Morello 3rd AP, Majmundar H, Thomas JJ, Sampson CH, et al. Technetium 99m sestamibi myocardial perfusion imaging predicts clinical outcome in the community outpatient setting. The Nuclear Utility in the Community (NUC) Study. *J Am Coll Cardiol*. 2004;43(2):213–23.
- Carro I, Cowie MR, Yamazaki J, Udelson J, Camici PG. Cardiac sympathetic imaging with mIBG in heart failure. *JACC Cardiovasc Imaging*. 2010;3(1):92–100.
- Morozumi T, Kusuoka H, Fukuchi K, Tani A, Uehara T, Matsuda S, et al. Myocardial iodine-123-metaiodobenzylguanidine images and autonomic nerve activity in normal subjects. *J Nucl Med*. 1997;38(1):49–52.
- McGhie AJ, Corbett JR, Akers MS, Kulkarni P, Sills MN, Kremers M, et al. Regional cardiac adrenergic function using I-123 meta-iodobenzylguanidine tomographic imaging after acute myocardial infarction. *Am J Cardiol*. 1991;67(4):236–42.
- Bengel FM, Barthel P, Matsunari I, Schmidt G, Schwaiger M. Kinetics of 123I-MIBG after acute myocardial infarction and reperfusion therapy. *J Nucl Med*. 1999;40(6):904–10.
- Simoes MV, Barthel P, Matsunari I, Nekolla SG, Schomig A, Schwaiger M, et al. Presence of sympathetically denervated but viable myocardium and its electrophysiologic correlates after early revascularised, acute myocardial infarction. *Eur Heart J*. 2004;25(7):551–7.
- Matsunari I, Schricke U, Bengel FM, Haase HU, Barthel P, Schmidt G, et al. Extent of cardiac sympathetic neuronal damage is determined by the area of ischemia in patients with acute coronary syndromes. *Circulation*. 2000;101(22):2579–85.
- Bax JJ, Kraft O, Buxton AE, Fjeld JG, Parizek P, Agostini D, et al. 123I-mIBG scintigraphy to predict inducibility of ventricular arrhythmias on cardiac electrophysiology testing: a prospective multicenter pilot study. *Circ Cardiovasc Imaging*. 2008;1(2):131–40.
- Gimelli A, Liga R, Giorgetti A, Genovesi D, Marzullo P. Assessment of myocardial adrenergic innervation with a solid-state dedicated cardiac cadmium-zinc-telluride camera: first clinical experience. *Eur Heart J Cardiovasc Imaging*. 2014;15(5):575–85.
- Bellevre D, Manrique A, Legallois D, Bross S, Baavour R, Roth N, et al. First determination of the heart-to-mediastinum ratio using cardiac dual isotope (123I-MIBG/99mTc-tetrofosmin) CZT imaging in patients with heart failure: the ADRECARD study. *Eur J Nucl Med Mol Imaging*. 2015;42(12):1912–9.
- Erlandsson K, Kacperski K, van Gramberg D, Hutton BF. Performance evaluation of D-SPECT: a novel SPECT system for nuclear cardiology. *Phys Med Biol*. 2009;54(9):2635–49.
- Leo W. *Techniques for nuclear and particle physics experiments*. 2nd ed. Berlin: Springer; 1994.
- Visser JJ, Sokole EB, Verberne HJ, Habraken JB, van de Stadt HJ, Jaspers JE, et al. A realistic 3-D gated cardiac phantom for quality control of gated myocardial perfusion SPET: the Amsterdam gated (AGATE) cardiac phantom. *Eur J Nucl Med Mol Imaging*. 2004;31(2):222–8.
- Bocher M, Blevis IM, Tsukerman L, Shrem Y, Kovalski G, Volokh L. A fast cardiac gamma camera with dynamic SPECT capabilities: design, system validation and future potential. *Eur J Nucl Med Mol Imaging*. 2010;37(10):1887–902.
- Lin L. A concordance correlation coefficient to evaluate reproducibility. *Biometrics*. 1989;45(1):255–68.
- Morgan CJ, Aban I. Methods for evaluating the agreement between diagnostic tests. *J Nucl Cardiol*. 2016;23(3):511–3.
- Landis JR, Koch GG. The measurement of observer agreement for categorical data. *Biometrics*. 1977;33(1):159–74.
- Jacobson AF, Senior R, Cerqueira MD, Wong ND, Thomas GS, Lopez VA, et al. Myocardial iodine-123 meta-iodobenzylguanidine imaging and cardiac events in heart failure. Results of the prospective ADMIRE-HF (AdreView Myocardial Imaging for Risk Evaluation in Heart Failure) study. *J Am Coll Cardiol*. 2010;55(20):2212–21.
- Imbert L, Poussier S, Franken PR, Songy B, Verger A, Morel O, et al. Compared performance of high-sensitivity cameras dedicated to myocardial perfusion SPECT: a comprehensive analysis of phantom and human images. *J Nucl Med*. 2012;53(12):1897–903.
- Bailliez A, Lairez O, Merlin C, Piriou N, Legallois D, Blaire T, et al. Left ventricular function assessment using 2 different cadmium-zinc-telluride cameras compared with a gamma-camera with cardiofocal collimators: dynamic cardiac phantom study and clinical validation. *J Nucl Med*. 2016;57(9):1370–5.

23. Kumita S, Cho K, Nakajo H, Toba M, Kijima T, Mizumura S, et al. Simultaneous assessment of Tc-99m-sestamibi and I-123-BMIPP myocardial distribution in patients with myocardial infarction: evaluation of left ventricular function with ECG-gated myocardial SPECT. *Ann Nucl Med*. 2000;14(6):453–9.
24. Ouyang J, Zhu X, Trott CM, El Fakhri G. Quantitative simultaneous 99mTc/123I cardiac SPECT using MC-JOSEM. *Med Phys*. 2009;36(2):602–11.
25. Ogawa K. Simulation study of triple-energy-window scatter correction in combined TI-201, Tc-99m SPECT. *Ann Nucl Med*. 1994;8(4):277–81.
26. Abdulghani M, Duell J, Smith M, Chen W, Bentzen SM, Asoglu R, et al. Global and regional myocardial innervation before and after ablation of drug-refractory ventricular tachycardia assessed with 123I-MIBG. *J Nucl Med*. 2015;56 Suppl 4:52S–8S.
27. Gimelli A, Liga R, Genovesi D, Giorgetti A, Kusch A, Marzullo P. Association between left ventricular regional sympathetic denervation and mechanical dyssynchrony in phase analysis: a cardiac CZT study. *Eur J Nucl Med Mol Imaging*. 2014;41(5):946–55.
28. Kacperski K, Erlandsson K, Ben-Haim S, Hutton BF. Iterative deconvolution of simultaneous 99mTc and 201TI projection data measured on a CdZnTe-based cardiac SPECT scanner. *Phys Med Biol*. 2011;56(5):1397–414.
29. Fan P, Hutton BF, Holstenson M, Ljungberg M, Hendrik Pretorius P, Prasad R, et al. Scatter and crosstalk corrections for (99m)Tc/(123)I dual-radionuclide imaging using a CZT SPECT system with pinhole collimators. *Med Phys*. 2015;42(12):6895.
30. Holstenson M, Erlandsson K, Poludniowski G, Ben-Haim S, Hutton BF. Model-based correction for scatter and tailing effects in simultaneous 99mTc and 123I imaging for a CdZnTe cardiac SPECT camera. *Phys Med Biol*. 2015;60(8):3045–63.

Submit your manuscript to a SpringerOpen[®] journal and benefit from:

- ▶ Convenient online submission
- ▶ Rigorous peer review
- ▶ Immediate publication on acceptance
- ▶ Open access: articles freely available online
- ▶ High visibility within the field
- ▶ Retaining the copyright to your article

Submit your next manuscript at ▶ springeropen.com
